SISSA - SCUOLA
INTERNAZIONALE
SUPERIORE
STUDI AVANZATI
TRIESTE
Strada Costiera 11

ISAS - INTERNATIONAL SCHOOL FOR ADVANCED STUDIES

Thesis submitted for the degree

of

"MAGISTER PHILOSOPHIAE"

"MOLECULAR DYNAMICS STUDIES OF SURFACE PHONONS"

Candidate

Wang Xiaoqian

Supervisor

Prof. Erio Tosatti

Academic Year 1986/87

TRIESTE

MOLECULAR DYNAMICS STUDIES OF SURFACE PHONONS

Acknowledgements

I would like to express my deep gratitude to Prof. E.Tosatti for his earnst and patient instructions and for his constant encouragement throughout the course of this study.

I am grateful to Dr.F.Ercolessi and Dr. G.L.Chiarotti for their help in endless discussions, for their collaborations, as well as their kind help in computer programs and critical reading of this thesis.

I wish to express my appreciation for Dr.A.Fasolino and Dr.C.Z.Wang for useful discussions.

I wish to thank A.Nobile and his staff for the enomous efforts spent to provide for a good computing enviroment among objective difficulties and all the other people who have contributed ideas and helped to complete this project.

Chapter 1

Introduction

Surface vibrations are involved in many processes on surfaces at ambient or elevated temperatures. A detailed knowledge of the surface-phonon spectrum is essential in studies of surface diffusion, phase transition on clean and adsorbate-covered surfaces, and desorption processes. It is also indispensable for any quantitative studies of energy transfer and dissipation at surfaces. Furthermore, the frequences of vibrational modes associated with adsorbed species can yield information on surface-adsorbate bonding, the geometry of the adsorption sites, and the lateral coupling between neighboring atoms or molecules on the surface.

The past few years have witnessed a rapid growth in the experimental effort to measure surface vibrations [1]. Development of experimental techniques in electron energy-loss spectroscopy [2-3] and inelastic He scattering [4-5] have reached such a stage of sophistication that reliable surface-phonon dispersion curves have been measured for a number of surfaces and data on many other interesting surfaces will become available in the near future.

There is a need for theory to interpret these results and to provide insights into the nature of the interatomic forces at the surface.

Surface-phonon dispersion curves for crystal surfaces can be obtained by solving for the vibrational modes of a slab or semi-infinite solid. Lattice-dynamics calculations [6] modeled the interatomic interactions by a Lennard-Jones potential. Subsequent studies [3-5] use more realistic force constants deduced from the fitting of measured phonon dispersion curves in the bulk, with empirical adjustments of the surface force constants to reproduce the measured frequencies of the surface modes. However, these changes in surface constants are quite sensitive to the models adopted for fitting the bulk phonons [7] and it is important to have realistic models to assess the magnitudes of these changes and their dependence on the surface geometry. Although the theory of lattice dynamics has been formulated for some time, it is well known that a detailed application of theoretical results to the experiments, especially for a complicated surface (e.g. in the presense of surface reconstructions), for temperature-dependent phase transitions and near melting, runs into formidable problems. This is particularly true for noble metals,where the d-s hybridization leads to many unusual properties of the system.

A way to cope with these problems is to introduce computer simulation techniques, but these, though exact in principle, are often still of low numerical accuracy, particularly molecular-dynamics results for $S(\mathbf{k},\omega)$. Furthermore, the surface phonons are much more complicated than that in the bulk case. While for the study of vibrational properties, MD is superior to standard lattice dynamics, particularly in that it accommodates, without any complications or approximations, for complex distortions, anharmonic

interactions and temperature effects, including possible diffusive motions and phase transitions.

This thesis is concerned with the molecular dynamics simulation of surface phonons. We show that with the calculation of time correlation functions, a detailed dispersion relation in a complicated slab system can be obtained. In our study of surface phonons on the Au(110) "missing row" reconstructed surface, unexpected high-frequency modes have been discovered based on many-body "glue" interactions. A detailed study of mode polarization and dipole activity shows that the highest mode, around 20meV, strongly modulates the first-third layer spacing, and should be observable in EELS experiments. A full study of temperature effects, including softening of high and low frequency surface modes, is also presented in this thesis.

The layout of the thesis is as follows:

Chap.2 describes the method, based on the MD simulation, to investigate surface phonon excitations. We have checked a simple test system Cu(100) and found an excellent agreement with the conventional lattice dynamics results.

Chap.3 contains an introductory review on the glue model and the static properties of the Au(110) reconstructed surface. Also the bulk phonon dispersion of gold has been calculated.

Chap.4 deals with our calculation of the surface phonon dispersion of the missing-row reconstructed Au(110) surface at various temperatures. The three main features of these results, namely high frequency modes,

low-frequency modes, and temperature dependence, are described.

In Chap.5 we calculated the electronic energy-loss spectroscopy, aiming at present an experimental detectable quantity for the observed anomalous high-frequency modes.

Chapter 2

Surface Phonons Studied by Molecular Dynamics

2.1 Molecular Dynamics Method

The molecular dynamics (MD) method was first applied by Alder and Wainright [8] to investigate the properties of a classical hard sphere system. The method has by now been extensively used [9-11]. The reason for its popularity is quite simple: it is the most direct technique that can be used to calculate time-dependent properties of an arbitrary, classical many- body system.

MD consists of a brute-force solution to the N-body dynamics and provides complete dynamical information about the system under study. MD can also yield equilibrium properties, but the real value is in its ability to follow the actual trajectories of the molecules in the system. The Monte Carlo (MC) simulation method, in contrast, can only yield equilibrium properties.

Obviously, the MD equilibrium properties and time correlations for a specific model can be compared with experimental results and thus be used to assess the model. The MD method has also been used to generate results for simple theoretical useful models in order to aid in the development of the theory of time correlation functions. The level of detail provided by MD is essentially complete, so that we are in the position to determine molecular behavior in condensed matter from first principles for a given model of molecular interaction.

Having assigned the positions and orientations, we calculate the net force and torque on each intermolecular potential energy functions. With the positions, velocities and forces and torques specified, we can begin the numerical solution of the classical Newton equations of motion. During the first several hundred time steps the molecular velocities can be scaled to a preset value of temperature. This is the equilibrium state corresponding to a desired value of temperature. This is the equilibrium stage during which the initial velocities relax to their correct equilibrium distribution. After sufficient equilibration the equation of motion are solved without velocity rescaling, and the positions, velocities, and other properties are periodically dumped for later storage on magnetic tape.

MD simulations are customarily carried out under conditions that correspond to the microcanonical ensemble of statistical mechanics and it follows in our calculations throughout. That is, the total energy E, the number of particles N and the volume V are fixed. Methods for performing MD simulations in other ensembles, i.e. constant N,P,H where P and H are the pressure and enthalpy, have also been developed [12].

Often experimental measurements produce spectra in wavenumber and in frequency space $(\mathbf{k}, \omega)$ whereas simulation results are obtained in real space and time $(\mathbf{r}, t)$. The two sets of results are theoretically related through Fourier and Laplace transforms, and explicit comparisons between simulation, experiment and theoretical models can be made. In particular, the simulation can serve as a test of a model system in a comparison with experiment.

MD generates real time trajectories of molecules. The trajectories, which are stored on magnetic tape, are analyzed for the time correlation functions relevant to a given dynamical property. For a system with free z-motion and periodic boundary conditions in x and y direction, the $Q_{\|}$ vectors which can be studied in the simulation are restricted to have the values

$$Q_{\|} = 2\pi(\frac{n_x}{L_x}\mathrm{i} + \frac{n_y}{L_y}\mathrm{j}) \tag{2.1}$$

where n_x, n_y are integers. This is because the system is periodic, by construction, with side length L_x, L_y in the x and y (space frame) directions.

2.2 Method

For describing collective motions, the dynamic structure factor defined by

$$S(\mathbf{k}, \omega) = \frac{1}{2\pi N} \sum_{i,j} \int_{-\infty}^{\infty} < e^{-i\mathbf{k}\mathbf{R}_i(t)} e^{i\mathbf{k}\mathbf{R}_i(0)} > e^{i\omega t} dt \tag{2.2}$$

is the experimental quantity indicating such motions. In the harmonic approximation the scattering function for one-phonon processes is proportional to the Fourier transform of the longitudinal displacement-displacement

correlation function. When the frequency dependence of $S(\mathbf{k},\omega)$ exhibits sharp peaks, the frequency of these peaks, as a function of wave vector $\mathbf{k}$, defines a dispersion curve of elementary excitations in the system. This curve is called dispersion relation for the density fluctuation. It turns out that the longitudinal as well as the transverse Fourier components of the currents become the collective coordinates governing the phonon excitations in such a system.

In view of the relation between the displacement and velocity, one may expect that the velocity correlations as well exhibit oscillatory time behavior. Thus the phonon excitations can be traced out by studying their couplings. It turns out that in practice the velocity-velocity correlation functions are easier for calculation.

For a slab system, the surface phonon spectral function $G^{l,\kappa}_{\alpha\beta}(\mathrm{Q}_\parallel,t)$ defined as

$$G^{l,\kappa}_{\alpha\beta}(\mathrm{Q}_\parallel,\omega)=\int_{-\infty}^{\infty}\frac{dtexp(i\omega t)<v^{l,\kappa}_{\alpha}(\mathrm{Q}_\parallel,t)v^{l,\kappa}_{\beta}(-\mathrm{Q}_\parallel,0)>}{2\pi<v^{l,\kappa}_{\alpha}(\mathrm{Q}_\parallel,0)v^{l,\kappa}_{\beta}(-\mathrm{Q}_\parallel,0)>} \tag{2.3}$$

can be studied through the time-dependence of displacement-displacement or velocity-velocity correlations such as their α coordinate

$$u^{l,\kappa}_{\alpha}(\mathrm{Q}_\parallel,t)=N^{-1/2}\sum_i(r^{l,\kappa}_{i,\alpha}(t)-R^{l,\kappa}_{i,\alpha})exp(i\mathrm{Q}_\parallel \mathrm{r}^{l,\kappa}_{i,\alpha}(t)) \tag{2.4}$$

$$v^{l,\kappa}_{\alpha}(\mathrm{Q}_\parallel,t)=N^{-1/2}\sum_i v^{l,\kappa}_{i,\alpha}(t)exp(i\mathrm{Q}_\parallel \mathrm{r}^{l,\kappa}_{i,\alpha}(t)) \tag{2.5}$$

where $r_{i,\alpha}(\mathrm{t})$ and $R_{i,\alpha}$ are the instantaneous and equilibrium positions of κth ion in ith cell in the lth layer and α, β run over polarizations. For given $\mathrm{Q}_\parallel$ values which are accessible in the MD simulations, phonons can be classified by using their dominant polarization characteristic. We have

chosen the longitudinal (L), shear vertical (SV) and shear horizontal (SH) directions, where L and SH represent vibrations with polarization parallel to the plane, parallel and perpendicular to $Q_{\|}$, respectively, and SV represents vibrations with polarization perpendicular to the surface and $Q_{\|}$.

Dispersions of surface phonons can be obtained by peaks of the spectral function $G^1_{\alpha\alpha}(Q_{\|}, \omega)$ along the dominant polarization directions. In this way we can trace out the frequencies of the surface phonons, through study of the correlations of motions in the outermost layer. In addition, the study of correlations associated with vibrations in the other layers is helpful in understanding of the bulk-modes and surface resonances.

Before discussing in more detail the practical application to complicated surfaces, we study a test system, calculate the surface phonons and compare with the conventional lattice dynamics results.

2.3 Test System: Cu(100)

As a test case, we have studied the Cu(100) surface, modeled by the two-body nearest neighbor potential potential of Jayanthi, Fasolino and Tosatti [13] (Fig.2.1). Since the Cu(100) surface under the potential is an ideal, unreconstructed surface and its MD has been well tested [13] , it is a suitable test system for our study.

To evaluate surface phonons one should in principle deal with a semi-infinite medium. This is actually true for long wavelength surface acoustic phonons [13] for which the penetration depth is very large. In this manner one avoids the interference effects occurring between the modes of the two

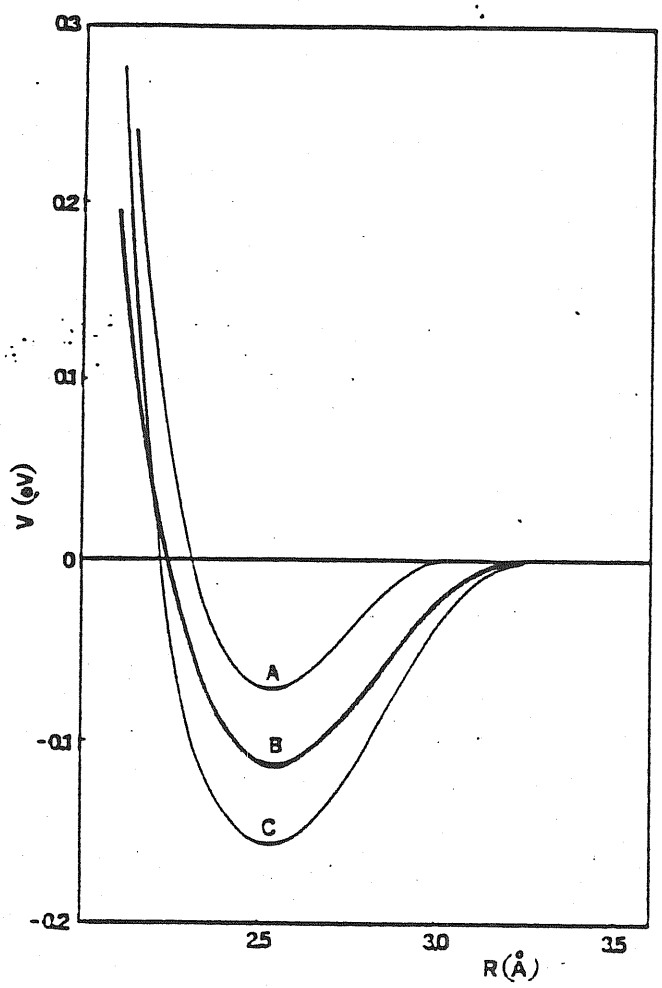

Fig.2.1. Pair potential (C) for copper used in our calculation.

surfaces present in a finite slab. The case of a semiinfinite crystal makes the theory very complicated. However we can treat the crystal as a slab containing a limited number of atomic planes and in the case that the slab is thick enough, the slab method gives a reasonable description of the surface phonon spectrum.

A necessary ingredient in the lattice-dynamical calculations for the bare surface is a proper description of the interatomic forces. For Cu substrates an accurate description is achieved by the nearest-neighbor central-force-constant JFT model for the phonon dynamics. In this model there is only one parameter β which is adjusted to fit the measured bulk-phonon spectra. More sophisticated models of the phonon dynamics for Cu exist which account for second-neighbor and angle-bending interactions [13]. Incorporation of these extra terms in the phonon dynamics only affected the surface-mode frequencies a few percent. This results from the fact that the angle- bending and second-neighbor force constants are $< 10\%$ of the nearest- neighbor force constant. Thus the single-parameter JFT model is adopted in our test calculations for its accuracy and simplicity.

In modeling the surface force constants, we use the truncated crystal approximation, where the loss of coordination of the surface force atoms is the only effect considered in determining the surface force constants. Thus the surface force constants are determined uniquely by the bulk values.

Using the nearest-neighbor central-force-constant model, the evaluation of the dynamical matrix for the fcc (100) surface is straightforward. The only nonzero matrices $D^{l,l'}_{\alpha\beta}(\mathrm{Q}_{\|})$ are those for $l = l', l' = l + 1$ and $l' = l - 1$. By evaluating those 3x3 bulk matrices and in a similar way

the 3x3 surface matrices using a truncated crystal, where the loss in coordination of the surface atoms is the only effect considered, the surface eigenmodes and eigenvectors for the finite slab with N atomic layers is then obtained by constructing the 3Nx3N dynamical matrix from the 3x3 submatrices . Once the dynamical matrix is formed, standard algorithms are used to solve the eigenvalues and eigenvectors.

The 3N eigenvalues $\omega_j(Q_{\|})$ for $Q_{\|}$ along the symmetry lines of the two dimensional Brillouin zone of the (100) surface of an fcc crystal, are sketched in Fig.2.2. There are frequencies associated with traveling modes which form a quasi continuum and frequencies associated with localized modes lying in energy gaps. The states decaying into the crystal are the surface states. Among them there is the Rayleigh wave whose frequency are the surface states formed by traveling and localized waves, the so-called resonant modes. By increasing the number of planes, the quasicontinuum of states becomes a continuum, that is the bulk phonon spectrum projected on the surface.

For the purpose of compare with the future MD calculation, in Fig.2.3 we show the corresponding surface phonon dispersions of a 6-layer slab. Of course in this case the bulk band can only be modeled by several modes and the surface modes at long wavelength are influenced by the interference effects.

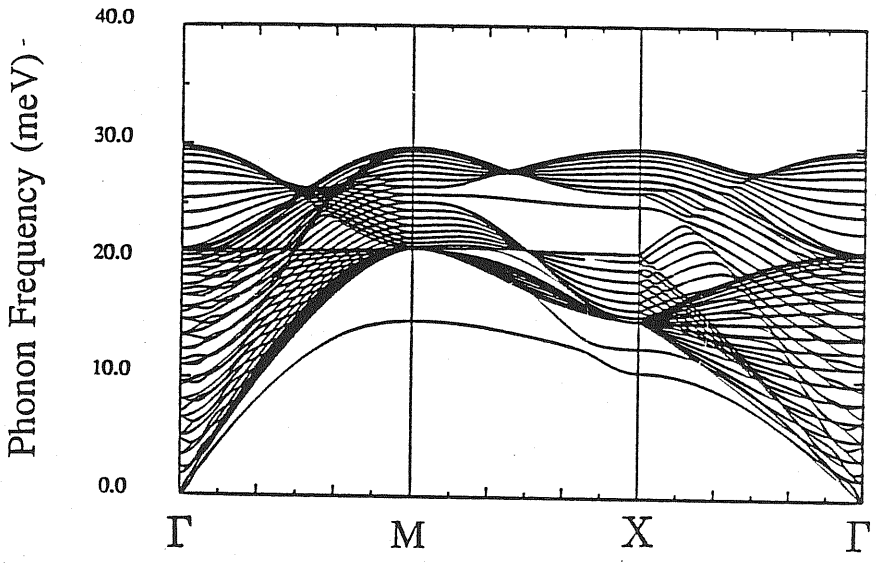

Fig.2.2. Surface Phonons of Cu(100), calculated by lattice dynamics with a 21-layer slab.

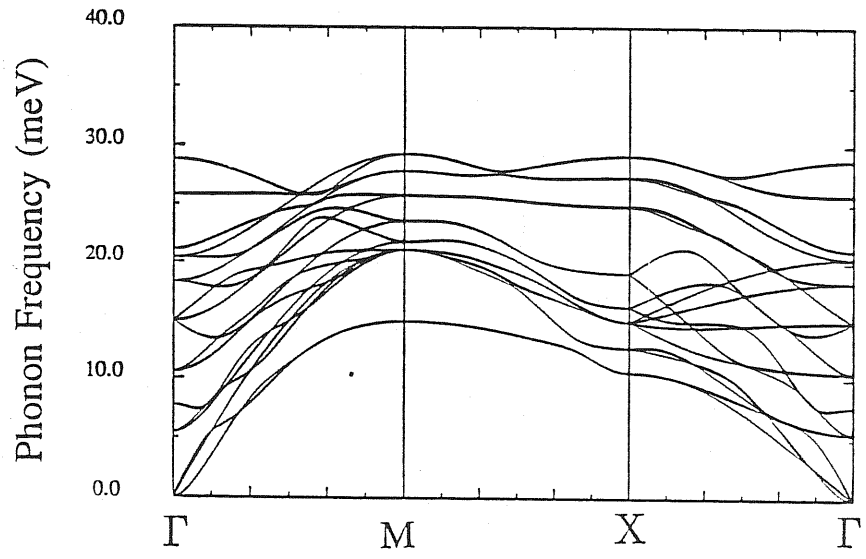

Fig.2.3. Surface Phonons of Cu(100), calculated by lattice dynamics with a 6-layer slab.

2.4 Results and Discussions

We choose a six layer slab and show in Fig.2.4, for system at room temperature, the velocity correlation spectrum for two (arbitrarily) chosen $Q_{\|}$-values along the segment ΓM of the two dimensional Brillouin zone. The conventional LD results at the same $Q_{\|}$ point are shown in the top panel of Fig.2.4, which is based on the same model. For $Q_{\|}$ values which are fit into the MD box, the overall agreement between the peak positions in the spectrum calculated by MD and the surface phonon dispersions is quite good. In addition to the peak positions give the dispersions of the surface phonons, the width of peaks may give information on temperature effect. Temperature effects on the surface phonon spectrum are small but nonzero, already at 300K for the present potential.

As a check, we have verified that the velocity-velocity correlation spectrum is proportional to ω^2 times the displacement-displacement correlation spectrum, which we calculate independently.

Temperature-fluctuations and surface relaxations appear to produce shoulders on these peaks or double peak structures as shown in Fig.2.4b , the S_1 mode at M point. For the purpose to avoid such a problem, in the future calculations we smooth the spectrum by replacing the δ -function like peak by a broadened peak with finite width.

We conclude that the present method provides a good quantitative way of calculating surface phonons. We may now use the method to explore other situations, including complicated surface reconstructions and temperature-dependent cases.

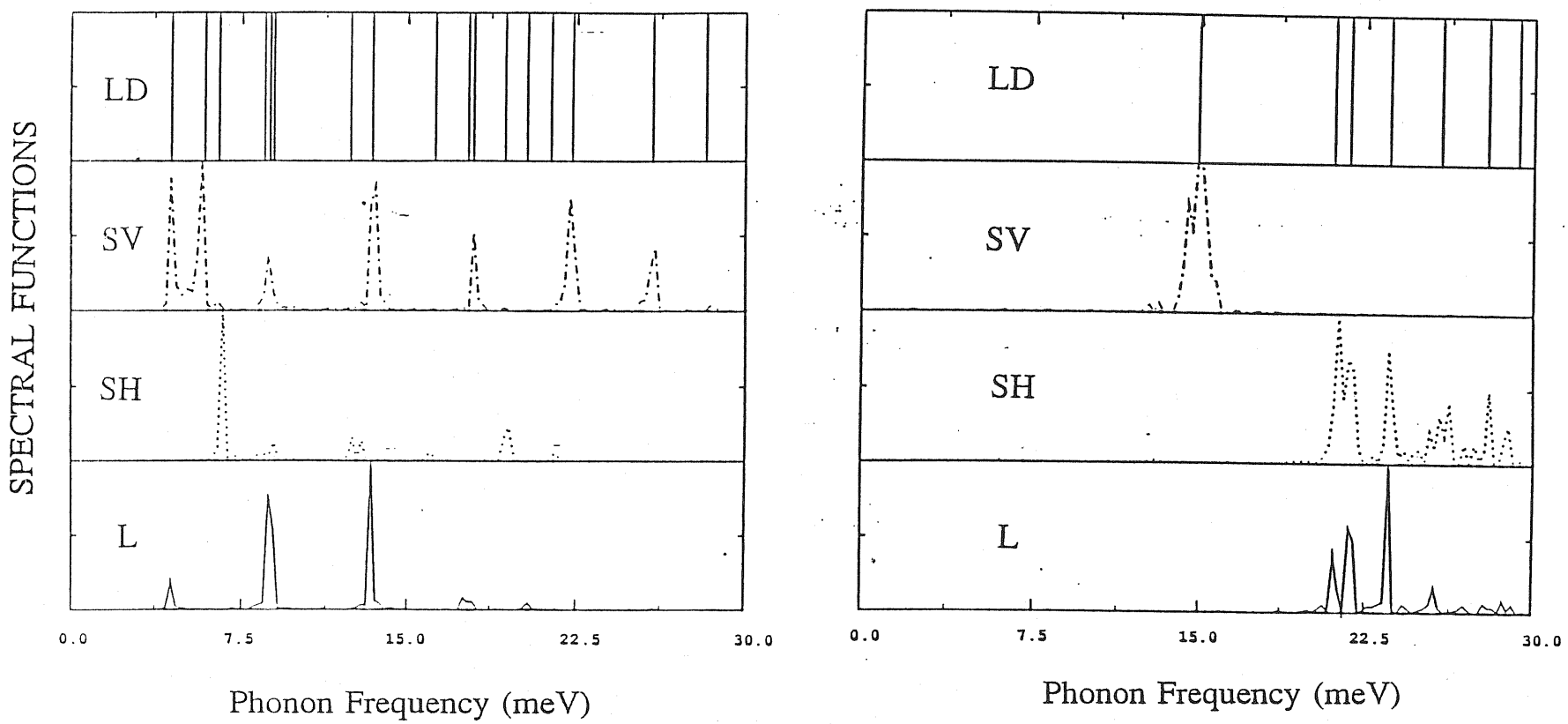

Fig.2.4. Surface phonon spectral functions

at two differen k-points.

Chapter 3

The Glue Model

3.1 Introduction

Many problems in solid-state physics and materials science require a detailed understanding of the energetics and structure of nonuniformities in metals and alloys. Due to the lower symmetry and long-range strains generally found around defects and surfaces, the study of these problems requires techniques that can handle a large number of atoms. This, in turn, requires a model of a solid which is both accurate and computationally simple. Historically, these problems have been addressed with various pair-potential models of the energetics of the constituents of the solid [14-16]. This approach is certainly useful in many circumstances. Pairwise interactions, however, fail very badly when applied to bulk noble metals, and are understandably even worse for their surfaces. The reason for this is electronic cohesion, which is strongly non-local and hence cannot generally be accounted for by pair, or even few-body, forces [17]. Noble metals like Cu, Ag and Au, which possess a (nearly) filled outer electronic d shell [18]

and about one sp valence electron, have very low shear elastic constants, $(c_{11} - c_{12})/2$ and c_{44}, as well exhibit large deviations from the Cauchy relation ($c_{12} = c_{44}$). The latter indicates the importance of many-body forces. Microscopically, electronic cohesion in a noble metal is due partly to the outer s-electron, and largely to the filled, but very broad, d-bands. This latter part is expected to be very non-directional in nature, since (crudely) the same d-bandwidth could equally well be produced by several well-spaced neighbours, or by fewer close-by neighbours. Based on this qualitative reasoning, improved phenomenological classical schemes, containing many-body forces, have been devised recently by several groups [18-22]. These schemes have been shown to be able to mimic the true lattice properties of noble metals [22] and bcc transition metals [20] very much better than pairwise forces. Ercolessi,Tosatti and Parrinello [19] have recently devised and optimized one such scheme, named the "glue" model, which is capable of accounting at the same time for both bulk and surface structural and thermal properties of Au. As with pair-potential models, the energetics of an arbitrary arrangement of atoms can be calculated quickly, but the ambiguity of the volume dependence inherent in pair-potential models [22] is avoided. Because the glue model provides a more realistic description of the metallic cohesion, it appears to be a desirable alternative to pair-potential models.

3.2 The glue scheme for gold

Since the advent of the earliest experimental tools in surface physics, the noble metal surfaces have constituted a kind of standard testing ground.

Their rather peculiar structural properties have therefore been discussed for a long time [23]. For iridium, platinum and gold, in particular, the most notable feature is surface reconstruction, namely a surface rearrangement which produces new strange surface periodicities. For example, the (110) surfaces all exhibit a so-called (1×2) reconstruction, meaning that the surface periodicity is twice as long as expected along one surface direction (the [001]), while it remains regular along the orthogonal $[\bar{1}10]$ direction.

A common factor of surface reconstructions seems to be the formation of close-packed (111)-type facets or overlayers, as was guessed pretty early in some cases [18,22]. The electronic motivation for this tendency is a subject of current theoretical research, and still open to discussion [24,25]. First-principle approaches (of the LDA type) are beginning to appear [24], but it will be presumably some time before a consensus based on them will form. In particular, it cannot be hoped that complicated geometries, such as those of the (100) or (111) surfaces, as well as the complex reconstruction/relaxation pattern of (110) reconstructed surfaces, could be handled without another breakthrough of the level of the recent Car-Parrinello method [11].

In the glue Hamiltonian, the total potential energy V of a system with N particles is written as

$$V = \frac{1}{2} \sum_{\substack{i,j=1 \\ (j \neq i)}}^{N} \phi(r_{ij}) + \sum_{i=1}^{N} U(n_i) \tag{3.1}$$

where

$$n_i = \sum_{\substack{j=1 \\ (j \neq i)}}^{N} \rho(r_{ij}) \tag{3.2}$$

and r_{ij} is the distance between atoms i and j. The three functions $\phi(r)$, $U(n)$ and $\rho(r)$ are built empirically. $\phi(r)$ is a standard short-range two-body potential, repulsive at small distances. n_i is a "generalized coordination" of atom i, computed as a sum of contributions $\rho(r_{ij})$ coming from the neighbouring atoms, $\rho(r)$ being a suitable positive, monotonically decaying short-range function. Finally, the "glue function" $U(n)$ associates an energy to this coordination.

It should be noted that: the units for n (and ρ) are arbitrary: they are only auxiliary quantities in the scheme. It is convenient to fix them by imposing $n_0 = 12$ where n_0 is the generalized coordination for a bulk atom in a perfect fcc lattice; a term which is linear in n can be assigned either to the two-body part or to the glue part. In fact, the glue Hamiltonian is invariant with respect to the transformation

$$\begin{array}{rcl} \phi(r) & \rightarrow & \hat{\phi}(r) = \phi(r) + 2\lambda\rho(r) \\ U(n) & \rightarrow & \hat{U}(n) = U(n) - \lambda n \end{array} \tag{3.3}$$

for any λ. Hence, with no loss of generality we can impose the condition

$$\left.\frac{dU}{dn}\right|_{n=n_0} = 0 \tag{3.4}$$

This choice is just a matter of convenience, since it simplifies the fitting process.

In the glue scheme, ϕ, U and ρ have been determined by fitting exactly the T=0 lattice parameter, the cohesive energy, the surface energy, the bulk modulus, and the transverse phonon frequency at the X-point [19,25]. Analytical forms based on polynomial splines have been used for all the functions, and the range of $\phi(r)$ and $\rho(r)$ have been arbitrarily limited to the first neighbours. The optimized functions are reproduced in Fig.3.1.

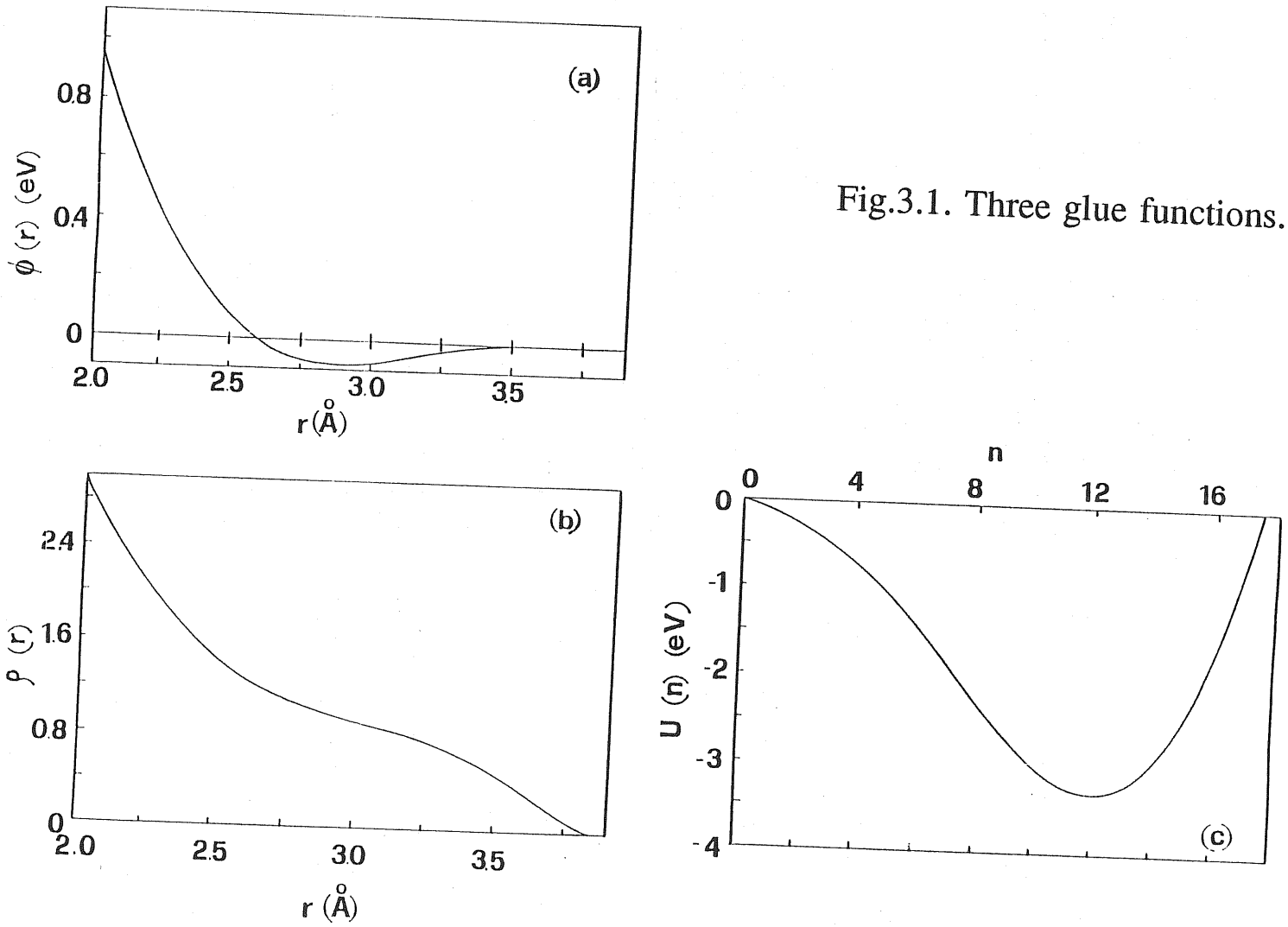

Fig.3.1. Three glue functions.

Quantity	*Experimental*	*Glue Model*
T=0 Lattice parameter (Å)	4.07	4.07*
Cohesive energy (eV/atom)	3.78	3.78*
Surface energy (meV/Å^2)	96.8	96.6*
Vacancy formation energy (eV)	0.95	1.26
Bulk modulus B (10^{12} dyne/cm^2)	1.803	1.803*
C_{11} (10^{12} dyne/cm^2)	2.016	2.203
C_{12} (10^{12} dyne/cm^2)	1.697	1.603
C_{44} (10^{12} dyne/cm^2)	0.454	0.600
Th. exp. coeff. at 773 K (10^{-6} K^{-1})	15.2	13.8*
Melting temperature (K)	1336	1357*
Latent heat of melting (eV/atom)	0.13	0.12
* fitted		

Table I: Comparison between some experimental quantities of gold and the same quantities as predicted by the glue model. The fit is not always exact, due to the procedure used (see text).

Table 3.1 compares calculated with experimental data for several properties of gold.

Computationally, the glue model energy can be evaluated with about the same amount of work as simple pair potentials since the forces depend only upon distances between pairs of particles. Therefore, it is still feasible to perform large-scale computer simulations of a wide variety of phenomena. Thus the glue hamiltonian provides a powerful new technique for atomistic calculations of metallic systems.

3.3 Bulk Phonons

With use of the parameters in our glue scheme, we calculate the bulk phonon dispersions. In Fig.3.2 we show the result. From discussions of the last section, we know that the X-point phonon has been fitted. As a consequence of the fitting process, the elastic constants (velocity of sound lines) associated with transverse modes are systematically higher than experimental results. While compared with the calculations with only two-body interactions, the glue potential improves results of elastic constants related with longitudinal modes. From the dispersion spectrum we can observe that the glue term does not have any effect on the transverse phonon frequencies: that are completely determined by the two-body potential. This fact can be intuitively understood by noting that the atomic density (or the coordination in the scheme) remains roughly constant in a transverse mode, while it is strongly modulated in a longitudinal mode.

It turns out that the many-body term in the expression for the bulk

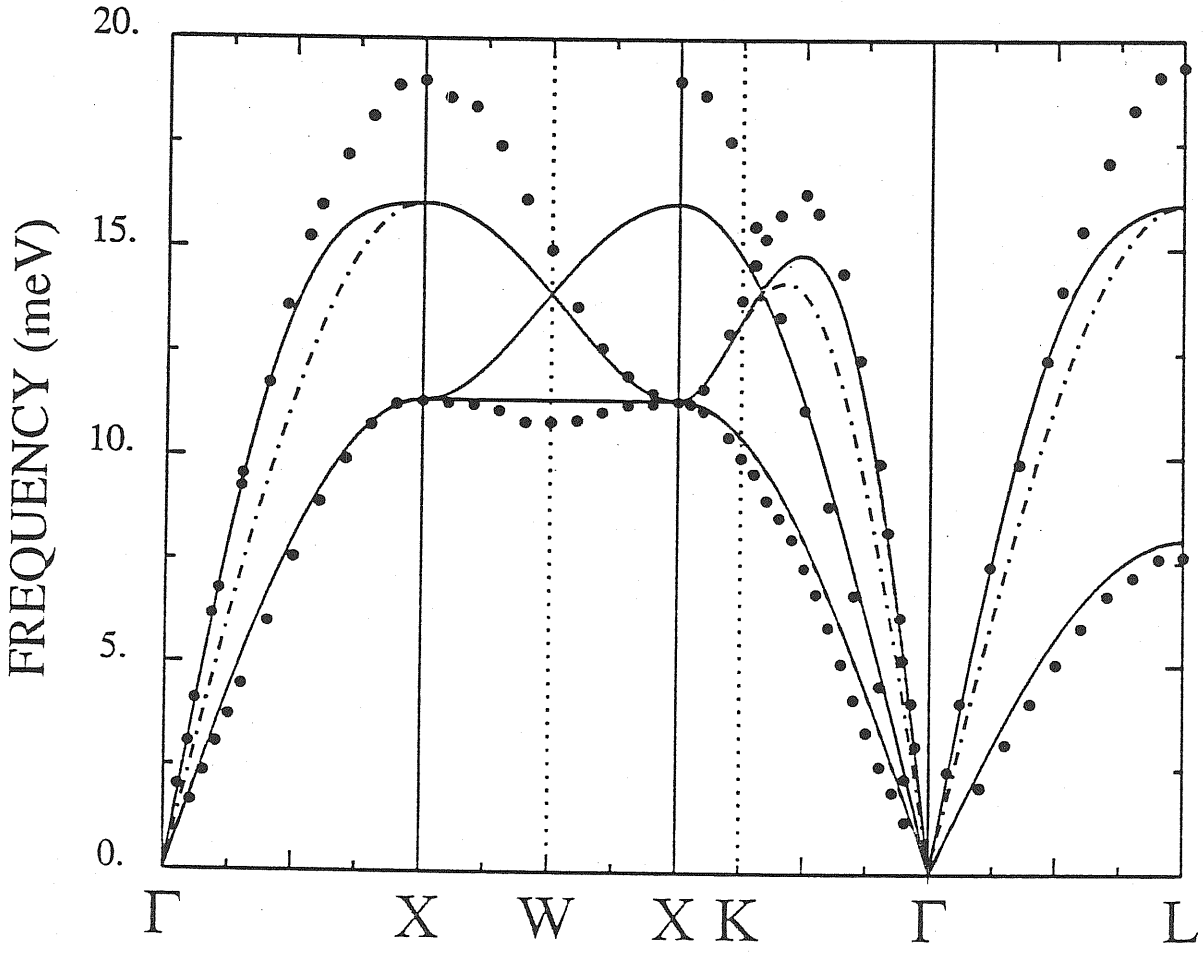

Fig.3.2. Bulk phonons calculated for Au in the glue potential.

modulus is what has been called "the Cauchy pressure". The glue hamiltonian removes the Cauchy discrepancy in the elastic constants. As stated above, the glue term does not have any effect on the transverse phonon frequencies. Moreover, it can be seen from the calculation that it does not have any effect for all $\bar{\mathbf{k}}$ points that lie on the Brillouin zone boundaries. Therefore, all the phonon frequencies at the standard points of the Brillouin zone can be expressed in terms of the two-body potential. All these frequencies, as well as the shear moduli, depend on a single parameter, namely $U''(12)$. Clearly, some kind of compromise must be adopted in the fitting process.

It follows from the results of the bulk phonon calculation that from the point of view of fitting the lattice vibration spectrum a glue hamiltonian is not substantially better than a two-body description. The origin of this difficulty lies in the fact that the glue is central, or non-directional, i.e. the glue energy depends only on the number of neighbours around an atom, while how these neighbours are disposed is not relevant. On the other hand, we expect that in real materials different angular arrangements of the atoms should make a significant difference to the energy. This picture is supported by the fact that it is possible to obtain an excellent agreement between the calculated and the experimental phonon dispersion relations by using three-body force constants with an angular dependence [22].

This spherical symmetry is perhaps the most important shortcoming of the glue hamiltonian when compared to other empirical many-body schemes. But, the simplification, resulting in a saving of computing power for a molecular dynamics or Monte Carlo simulation, is enormous, and can hardly be underestimated. However, we note that in the presence of surface

or defects, due to the lack of symmetry in z-direction or in the system, the terms containing

$$U''(n_j)\sum_i \rho_j R_{ij}^{\alpha}/R_{ij} \tag{3.5}$$

is no longer without contribution. In these cases the dynamical matrices depends delicately on the parameter $U''(n)$ where n is the coordination of the atoms. Since the coordination of atoms at surface are poor, the force constants at surface crucially depend on the geometry of the system and in reality the glue term provides naturally the driving force of reconstruction of surfaces.

3.4 Static Properties of Au(110)

The (110) surfaces of Ir, Pt and Au exhibit a (1×2) reconstruction, meaning that the surface unit cell length is the same as in a truncated bulk along the [$\bar{1}$10] direction, while it is twice as long along [001]. Among gold surfaces, Au(110) is probably the most studied. Experimental data for Au(110) have been obtained with a number of different techniques, namely LEED , He-diffraction , low, medium and high energy ion scattering, STM , X-ray diffraction and transmission electron microscopy [23].

While various models have been proposed in the past to explain the (1 × 2) pattern (see, e.g., Ref.[26]), general consensus has now gathered around the "missing row" model. In this model, every other close-packed [$\bar{1}$10] row is absent in the topmost layer. The resulting surface structure is thus constituted by a succession of tiny (111) facets, which form—neglecting relaxation effects—a 35° angle with the surface plane. A point debated in

literature concerns the relaxation of the top row. By now, most authors believe that the top (ridge) row is contracted towards the second layer [26,27], although expansion had been argued by some authors [22].

The $T = 0$ missing-row structure of Au(110) (1×2) as given by the glue model was detailed in ref.[23]. The topmost row is sunken by $\sim 27\%$, the second-layer rows are slightly inwards paired, and the third-layer buckling magnitude is about 26%. While experiments [28,29] indicate somewhat smaller relaxations, and no second-layer inwards pairing, the overall agreement of the distortion pattern seems fairly good. We also found a small (~ 0.2 Å) sliding distortion of the top rows along their own direction. The average distortion however disappears at an Ising-like critical temperature $T_c \sim 230K$.

Other theoretical studies [26,27] also predict stability of the Au(110) missing row structure, although they differ on the details of the relaxation geometry. On the other hand, a calculation made by Daw for the similar Pt(110) (1×2), using an Hamiltonian of the same class, shows directions of the atomic displacements in agreement with the study [25,26].

"Missing row" structures are found close in surface energy—just above the (1×2) and all well below the non-reconstructed (110). These structures differ from the (1×2) in the extension of the (111) facets: a $(1 \times n)$ missing row has $(n + 1)$-row wide slanted (111) facets. The (1×3) and (1×4) are occasionally observed experimentally Our data confirm that the tendency to (111) faceting is the driving force for the (110) reconstruction, as suggested by Binnig *et al.* [29].

All the relaxed structures, including the (1×1), exhibit a small slid-

ing distortion of the top rows along $[\bar{1}10]$, i.e., parallel to themselves (see the inset of Fig.3.3). On the optimal (1×2) missing row, this distortion amounts to 0.26 Å for the top row atoms and to 0.06 Å for the third layer atoms underneath. As a side effect, the mirror symmetry across a (100) plane (orthogonal to the rows) is destroyed. We are not sure for the time-being whether the true Au(110) should have a similar phase transition, or whether this is an artifact of our glue model. A room-temperature symmetry breaking which might be explained by our distortion was reported by spin-polarized LEED [30], but was later questioned by another group [31]. In our system these atom displacements form a sort of strongly anisotropic Ising-like system. The distortion order parameter disappears with a phase transition at $T_c \simeq 230$ K, where the full (average) symmetry of the surface is restored. Low-temperature diffraction studies of Au(110) would be helpful in settling this question.

Fig.3.3.

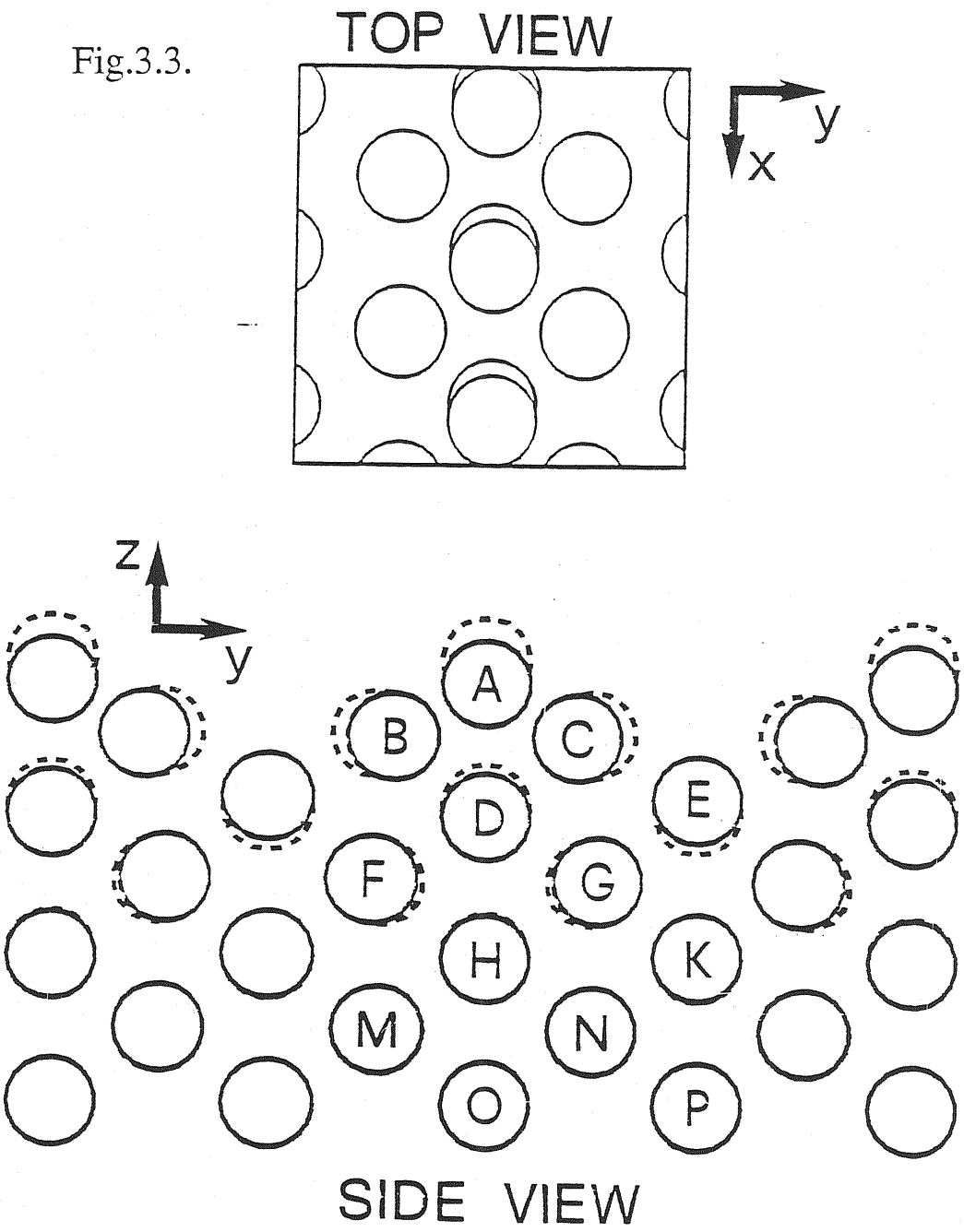

Chapter 4

Surface Phonons on the Missing-Row Reconstructed Au(110) in the Glue Model

The so-called "missing-row" reconstruction of noble metal (110) surfaces has been the subject of much attention. As discussed in last chapter, it is found on clean Au [28-30], Ir [30], Pt [31], while Cu and Ag are "dormant" cases—the reconstruction can be provoked by only a modest alkali coverage [32]. Through the removal of every other row the flat (110) surface is converted into a sequence of tiny (111) facets, which in turn are favoured by the very low (111) surface energy, relative to (110) [29]. Recent experimental studies of Au(110) (which we take as our prototype) have shown [27,28] that the reconstruction is accompanied by heavy distortions (multilayer relaxations) of the surface lattice, the second-layer rows are laterally displaced, and the third atomic plane also undergoes a large buckling distortion.

Theoretically, this type of reconstruction pattern has been shown to

yield a minimum of surface energy, both by first-principle electronic calculations [24], and by phenomenological many-body force schemes, such as the "glue" [19] or "embedded atom" [18] models. The latter approaches are particularly revealing in showing how both the reconstruction and the associated relaxation arise from the necessity of bringing the surface atom coordination as close as possible to the higher bulk value, at least to the extent permitted by hard-core repulsions.

Many implications of this complex reconstruction/relaxation pattern of the missing row surfaces on the surface dynamics are as yet unexplored. In particular, it could be expected that large distortions, such as the heavy sinking of the topmost rows, might bring about fairly heavy modifications of the surface phonon spectrum. In this chapter we present new theoretical evidence, predicting the existence of anomalous high-frequency modes as a typical signature of the missing-row reconstruction. We focus in particular on Au(110), which stands out so far as the best studied missing-row noble metal surface.

4.1 MD DETAILS

We investigate the dynamical behaviour of the missing-row reconstructed surface using MD. For the present dynamical study, we have used two different slab systems, denoted as A and B, each consisting of 1200 particles arranged in 16 layers, with 40 (1×2) unit cells on each free surface, plus in-plane periodic boundary conditions. System A has a rectangular 20×4 MD cell, i.e., the cell length is $20a/\sqrt{2}$ along the direction (henceforth direction x), and $4a$ along (henceforth direction y), where a is the lattice parameter

of the crystal. System B is instead elongated along y, with a 4×20 MD cell. We use A to compute the phonon frequencies along directions ΓX and YS in the surface Brillouin zone, and B for directions ΓY and XS. By comparing the two results at $\vec{k}$ points common to both systems, we have checked that size effects are negligible within our accuracy (better than 0.1meV).

Standard microcanonical MD is used, with a time step $\Delta t = 7.14 \times 10^{-15}$ s. The in-plane lattice parameter a is set at each temperature from a zero-pressure bulk calculation [22] with the same potential (values ranging from $a = 4.074\mathring{A}$ for T=50K to $a = 4.092\mathring{A}$ for T=500K). Approximate surface phonon spectral densities are extracted from the trajectories through the $\vec{k}$-resolved, first-layer velocity-velocity correlation functions as discussed in the previous chapters.

4.2 THE SURFACE PHONON SPECTRUM

The phonon spectrum is reported in Fig.4.1: dashed regions indicates the reconstructed surface projection of the bulk modes calculated with our potential using a standard lattice dynamics calculation (T=0K). At the edges of the bulk-phonon bands we may encounter Van Hove singularities. We can work out the surface projection of the bulk bands by using

$$\rho(Q_{\|}) = \sum_{k_z} \delta(\omega^2 - \omega_j^2) \tag{4.1}$$

then within the bulk-phonon bands we are left with a one-dimensional density of states, the density of the bulk phonons whose wave vector lies along a line in the three-dimensional Brillouin zone, normal to the surface. Such

Fig.4.1.

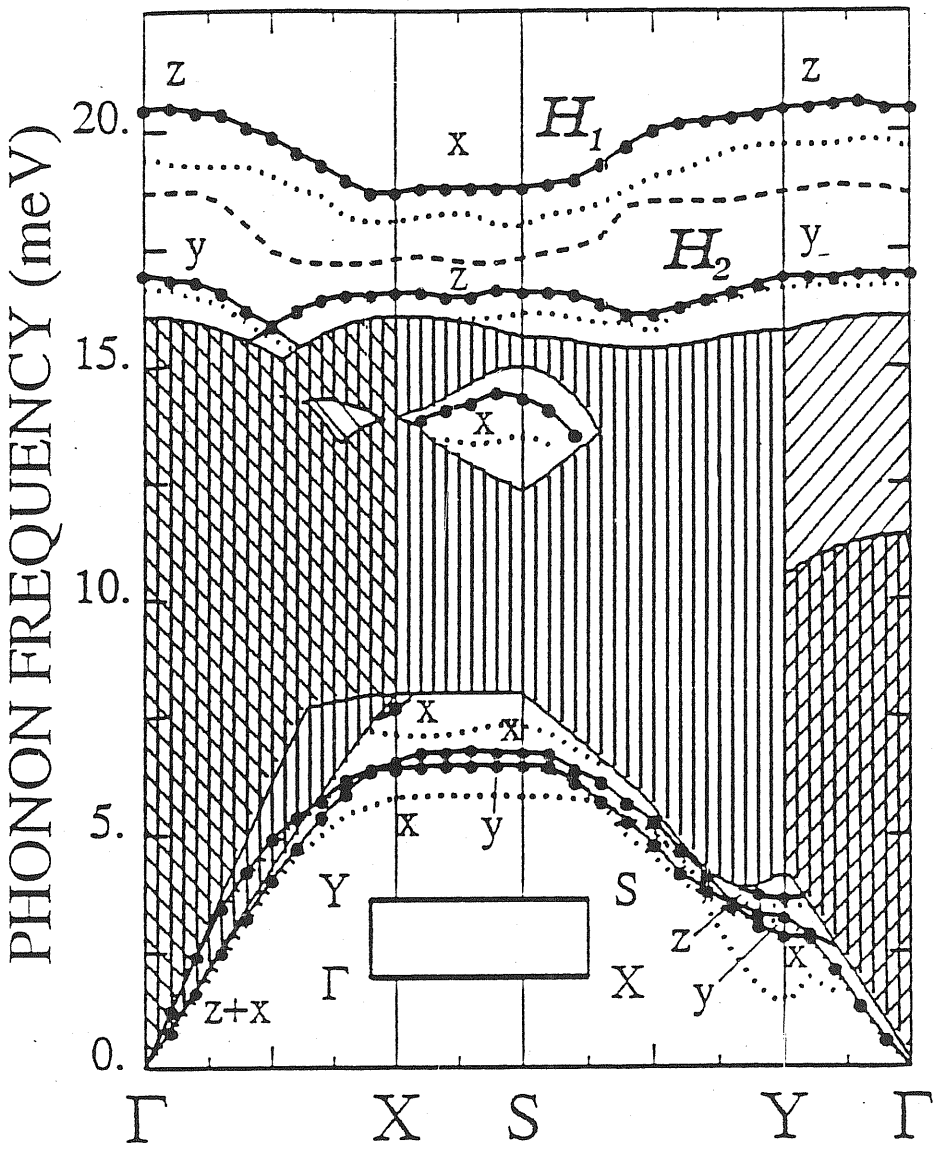

Phonon dispersion at $T = 50\,\mathrm{K}$ (solid lines), $T = 230\,\mathrm{K}$ (dotted lines), and $T = 500\,\mathrm{K}$ (dashed line). The shaded regions indicate surface-projected bulk modes at $T = 0$, from lattice dynamics. Crossing of different branches is allowed in the ΓX and SY directions, and avoided elsewhere below 230 K, due to the sliding distortion. Directions x, y and z denote in the order $\langle\bar{1}10\rangle$, $\langle 001\rangle$ and $\langle 110\rangle$ crystallographic directions, and $\Gamma = (0,0)$, $X = \frac{\pi}{a}(\sqrt{2},0)$, $Y = \frac{\pi}{a}(0,\frac{1}{2})$, $S = \frac{\pi}{a}(\sqrt{2},\frac{1}{2})$. At $T = 500\,\mathrm{K}$ only the highest frequency mode is shown, the others being in the bulk region or difficult to distinguish. The labels indicate the (main) polarization directions for several branches.

one-dimensional density of states have Van Hove singularities of the form $|\omega - \omega_c|^{-1/2}$ at the band edge with frequency ω_c.

Despite the considerable complexity of the surface-mode spectra shown above, all the surface modes and mixed modes can be understood in the context of a simple phenomenological scheme [6]. We begin with the bulk bands for a crystal without surfaces. For a monoatomic crystal there are ordinarily be three bands (which may overlap), corresponding roughly to two groups of transverse modes and one of longitudinal modes. We then introduce the perturbation represented by the surface, which actually consists of two parts-a "first order" perturbation due simply to the truncation of the crystal and a " second-order" perturbation due to changes in the force constants near the surface. At large wavelengths, where the surface modes penetrate deeply, the second part should not be important, but it is important at small wavelengths.

The strength of the total perturbation depends on the point in the SBZ. If the perturbation is strong enough for a given value of $Q_{\|}$, it will peel one or more surfacelike modes off a given bulk band. Ordinarily the perturbation should correspond to a softening of the vibrations, since the truncation of the crystal allows the surface atoms to vibrate more freely. For such a softening perturbation, the surface modes should be peeled off the bottom of the bulk band. It is interesting to note that , due to the missing row reconstruction, the coordination of atoms at top and second layers is poor,then the glue potential causes a change in the interaction between the particles near the surface, the total perturbation leads to a stiffening of the lattice vibrations. In such a case the surface modes are peeled off the top of the bulk band. Such high-frequency surface modes were produced in the

calculations of Musser and Rieder [6] when the surface force constants were stiffened, but it does not seem likely that they will occur naturally in ideal monoatomic crystals. We will discuss in next chapter about this mode in some detail.

Ordinarily, the total perturbation due to the surface should first peel off (from a given bulk band) a mode primarily localized in the first layer. If strong enough, it should then peel off a mode primarily localized in the second layer,and so on. The nth-layer mode in this series has the same character in the nth layer as the first-layer mode has in the first layer. Sometimes the perturbation will not completely succeed in peeling off the mode, in which case the mode remains within the bulk band as a mixed mode.

When a mode is peeled off, one of four things will happen: (a) It may fall under all of the bulk bands, in which case it will necessarily be a surface mode. (b) It may fall into a gap between two bulk bands, in which case it again will necessarily be a surface mode. (c) Along a symmetry line associated with a reflection plane, it may fall into a region occupied by bulk modes to which it is automatically orthogonal, as shown in Fig.4.1, the S_2 mode along ΓX direction. In this case it will necessarily be a surface mode. (d) It may fall into a region occupied by bulk modes to which it is not automatically orthogonal. In this case it will not be able to survive as a pure mode and will be a mixed mode instead.

Occasionally two surface-mode branches will attempt to cross each other. In such a case there will be hybridization, with the hybrid branches exhibiting a mutual repulsion and interchange of character. The only case

where two surface-mode branches could, in fact, cross is along a symmetry line associated with a reflection plane, with the two modes belonging to mutually orthogonal classes and therefore invisible to one another. Such a situation does occur in the present results along ΓX direction. While at higher temperatures, when the sliding-distortion has been averaged up, the crossing is allowed in the ΓY direction.

4.3 Discussions

We have constructed the phonon dispersion curves for T=50K, T=230K, and T=500K in Fig.4.1. The main feature of these results, namely high-frequency modes,low-frequency modes, and temperature dependence, will be seperately described below.

(i) *High-frequency modes.* The main striking feature of this spectrum consists of two anomalous high frequency surface modes with rather flat dispersion (H_1, around 20 meV, and H_2, around 17 meV). To clarify their origin, we have made a separate study of their eigenvectors by using the quench-echo technique [33]. If all atom velocities in the simulation are artificially set to zero with a frequency $2\omega_0$, only the vibrational modes of frequency ω_0, $2\omega_0$, ...,$n\omega_0$ survive, while all the others are destroyed. For high enough ω_0, there are no modes of $\omega = n\omega_0$ with $n > 1$, and single phonons can be studied. We have applied this procedure for $\omega_0 \simeq 20meV$ and $\omega_0 \simeq 17meV$. Due to the flat dispersion, several modes with nearly the same frequency but slightly different $\vec{k}$ vectors are excited. To single out the eigenvectors at one $\vec{k}$ point, we further calculate the Fourier-transform of the atomic displacements $\sum_m e^{i\vec{k}\cdot\vec{R}_m}\vec{u}_{ms}(t)$ ($\vec{u}_{ms}$ denoting displacements

of atom s in the cell m located at $\vec{R}_m$) and then retain only the desired $\vec{k}$-component.

The eigenvectors of H_1 and H_2 obtained in this way at $\vec{k} = 0$ are shown on Fig.4.2. In mode H_1, the top row atoms and the third-layer atoms just beneath move essentially along z (with a small x component, related to the sliding distortion), while the second-layer atoms move mainly along y with a small z component. These four atoms move essentially towards (or away from) their center of mass, thus clarifying the large stiffness of this mode. Third-layer atoms below the missing rows remain almost motionless. This form of the eigenvector indicates that this high-frequency mode arises because of the deep sinking of the topmost row, giving rise to a stiffening of surface force constants. In mode H_2, all motions are essentially along y, and only second-layer atoms exhibit some z component. This mode is very close to the bulk continuum, and might be difficult to detect in practice. Conversely, mode H_1 lies well above, and should be easily detectable, by either inelastic He-scattering or by electron-energy-loss spectroscopy (EELS), this will be confirmed in the next section.

From the above discussion one can realize that the glue force provides a source for the stiffening of the first-third layer force constants. The presence of strong inwards relaxations, quite typical of many metal surfaces (but not of LJ surfaces) may lead to a surface stiffening . A quantitative theoretical verification of the tendency of some metal is generally difficult, because of the complicated many-body nature of electronic forces. However gold should in many respects represent the opposite extreme as compared with metals which can be described by the conventional two-body forces. The necessity of improving surface close-packing is strong enough in gold

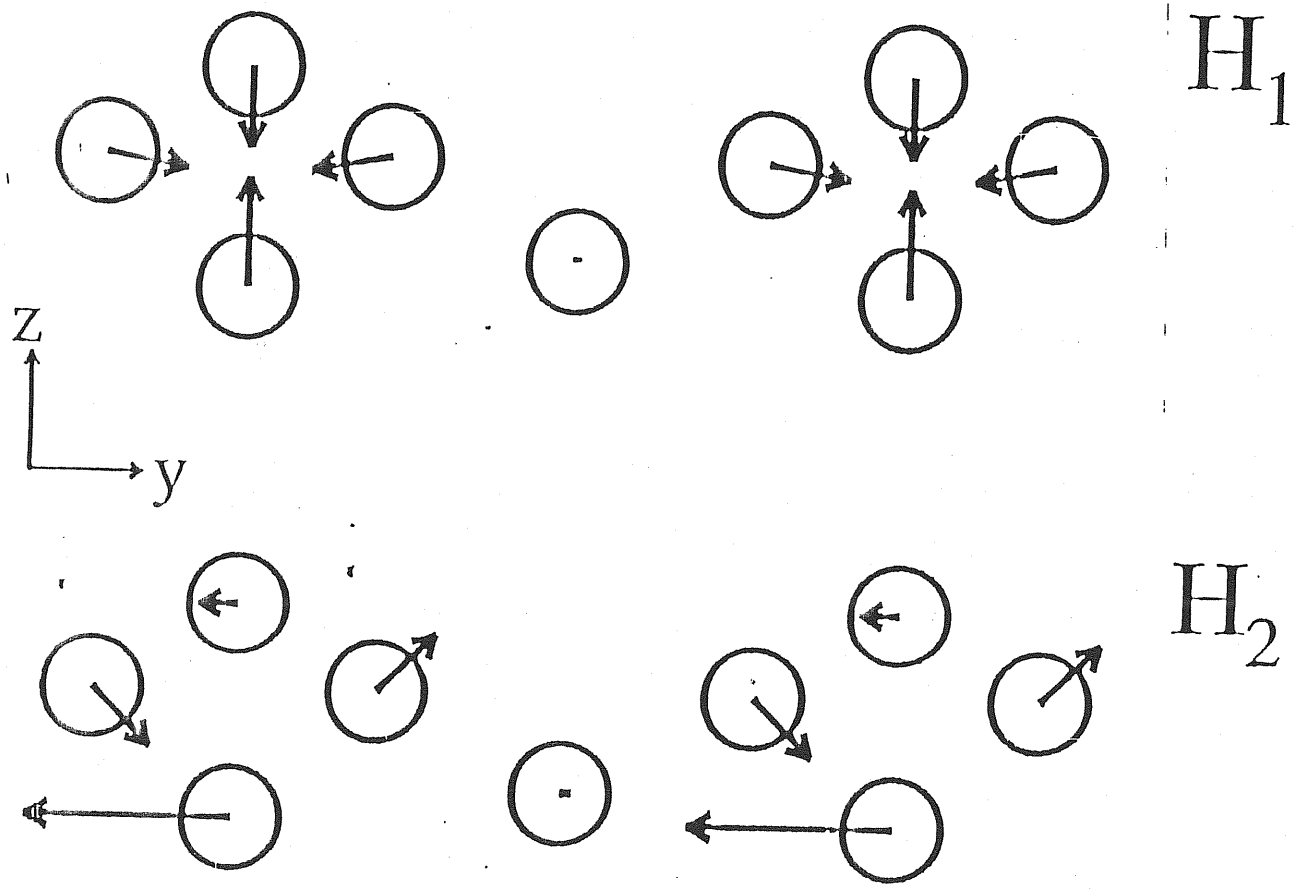

Fig.4.2. Atom displacements corresponding to the two high-frequency $\vec{k} = 0$ modes H_1 and H_2. The arrow length is proportional to the relative displacement. The first three layers of two unit cells are shown. In both modes, the third-layer atoms below the missing rows are almost at rest. In H_1, a small x motion of the top row is not shown.

to make simple inwards relaxation insufficient, causing instead a surface reconstruction phenomenon. The stiffening arises mainly because the reduced number of "bonds" of a surface atom (relative to a bulk atom) implies that each bond becomes shorter and stiffer. This, in turn, causes the surface lattice to be less prone to acquire both large anharmonic fluctuations, and large concentration of defects such as vacancies or adatoms.

(ii) *Low-frequency modes.* The low-frequency modes in Fig.4.1 have quite a normal appearance. In particular, we note that the "hindered translations" along y are not particularly soft. Again, this stiffness can be attributed to the deep top row sinking. Regular Rayleigh-like waves are found at small $\vec{k}$-vectors, somewhat more prominent along ΓY. As typical spectral functions, we collect our results at several high symmetry points. Fig.4.3a shows the results at Γ point. The two high frequency modes shift their frequencies toward the band edge. Fig.4.3b shows the results at Y point. It should be noted that the SH modes (vibrate along x-direction) soften near the critical temperature $T_c \simeq 230K$. Fig.4.3c shows the results at X point. The vibrations along x and z direction change much stronger than those along y-direction, and. Fig.4.3d shows the results at S point.

(iii) *Temperature dependence.* A temperature-dependence of the surface phonon spectrum can arise due to different reasons, namely (a) surface structural phase transitions; (b) intrinsic surface anharmonicity; (c) overall bulk anharmonicity. Our missing-row (110) surface has in principle two phase transitions, one connected with the sliding distortion ($T_c \sim 230K$) and another connected with the disappearance of reconstruction $(1 \times 2) \rightarrow (1 \times 1)$. The latter, experimentally found around $700K$ in Au [34-36], has recently been studied by Monte Carlo methods by Daw [37]. The present MD

Fig.4.3. SURFACE PHONON SPECTRAL FUNCTIONS (Arb. Un.)

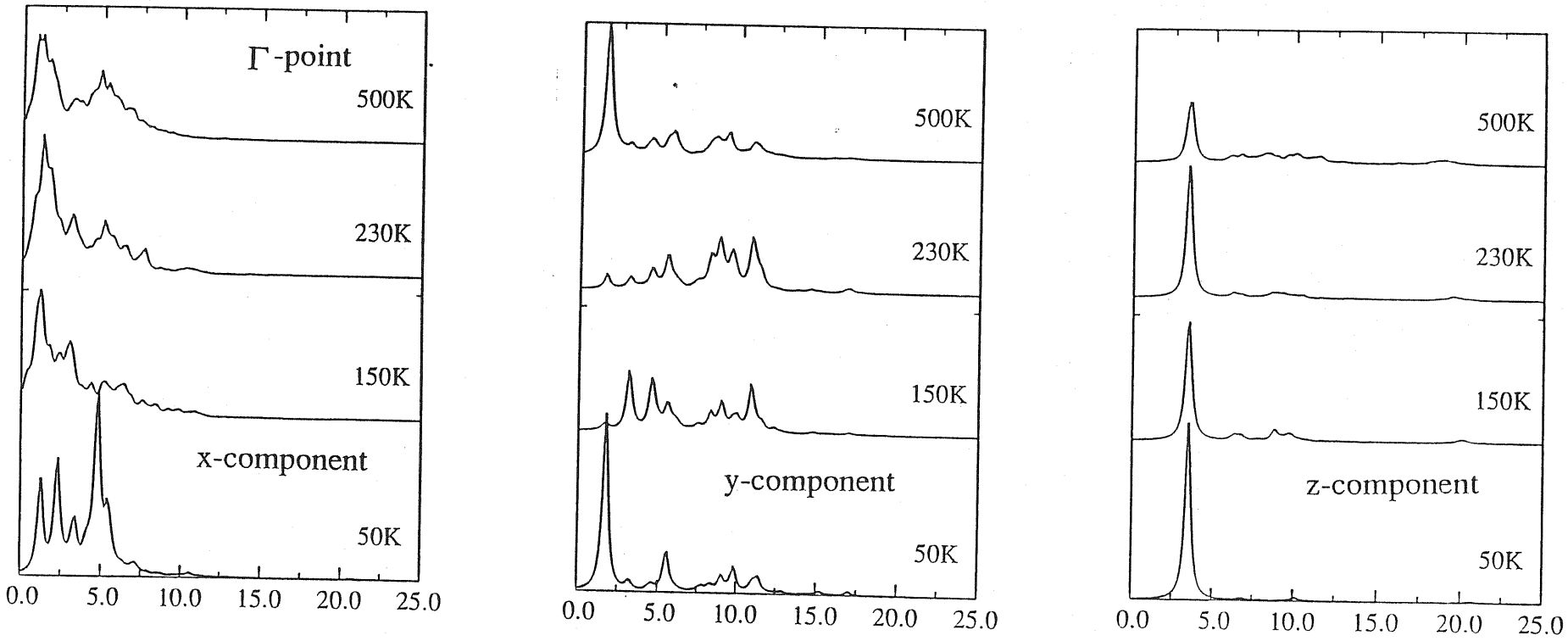

SURFACE PHONON SPECTRAL FUNCTIONS (Arb. Un.)

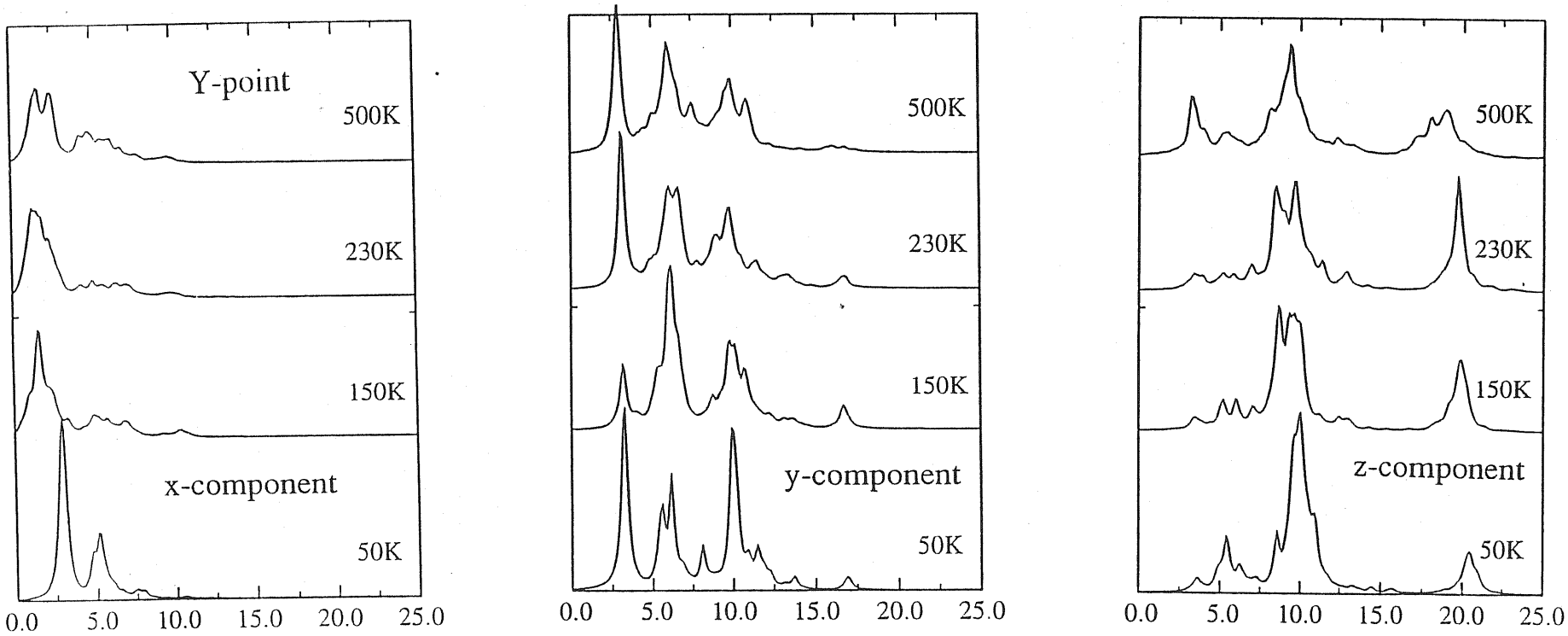

SURFACE PHONON SPECTRAL FUNCTIONS (Arb. Un.)

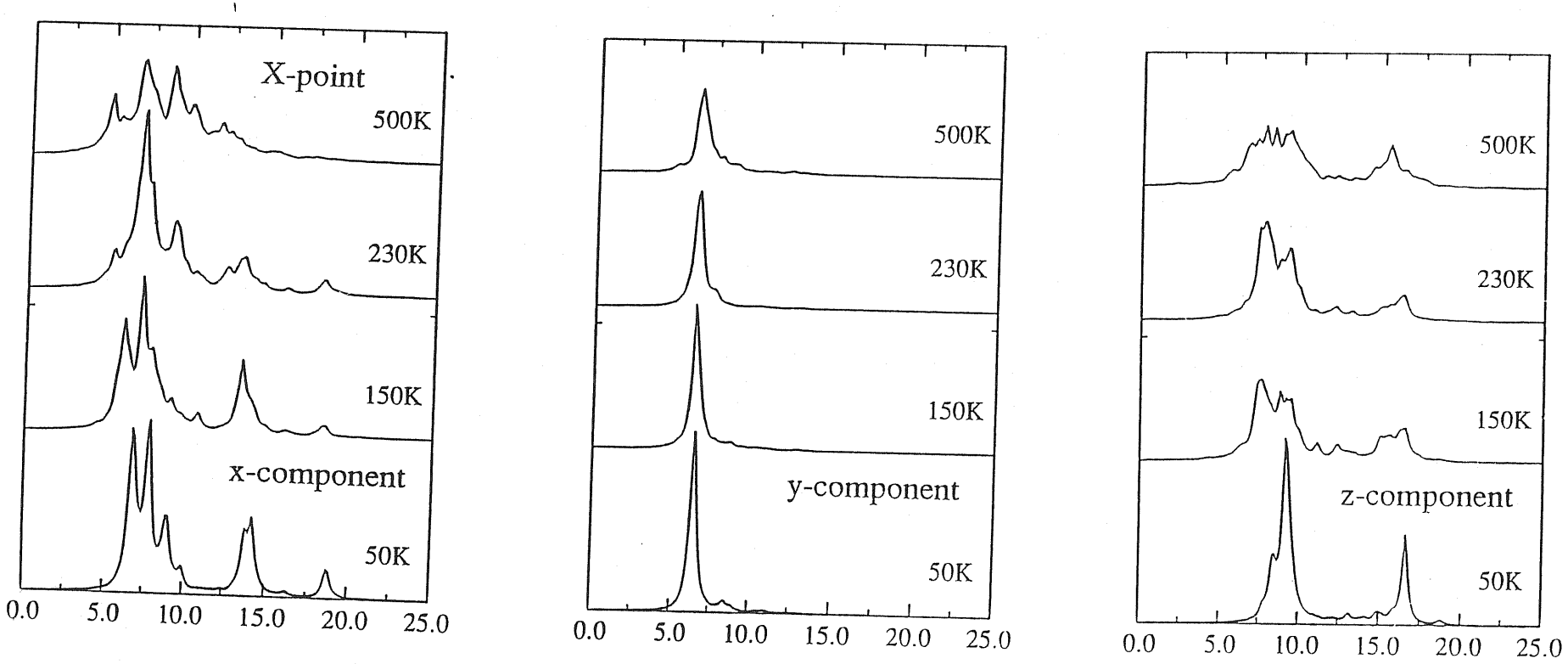

SURFACE PHONON SPECTRAL FUNCTIONS (Arb. Un.)

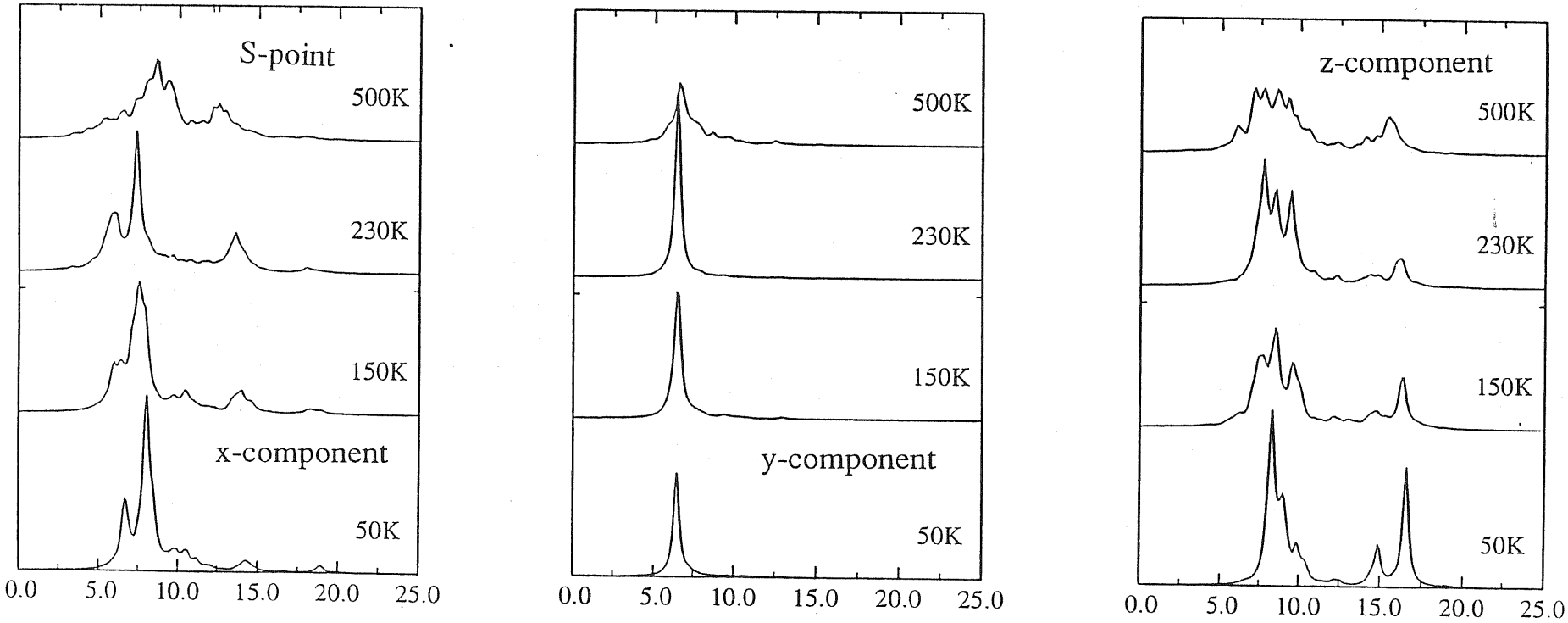

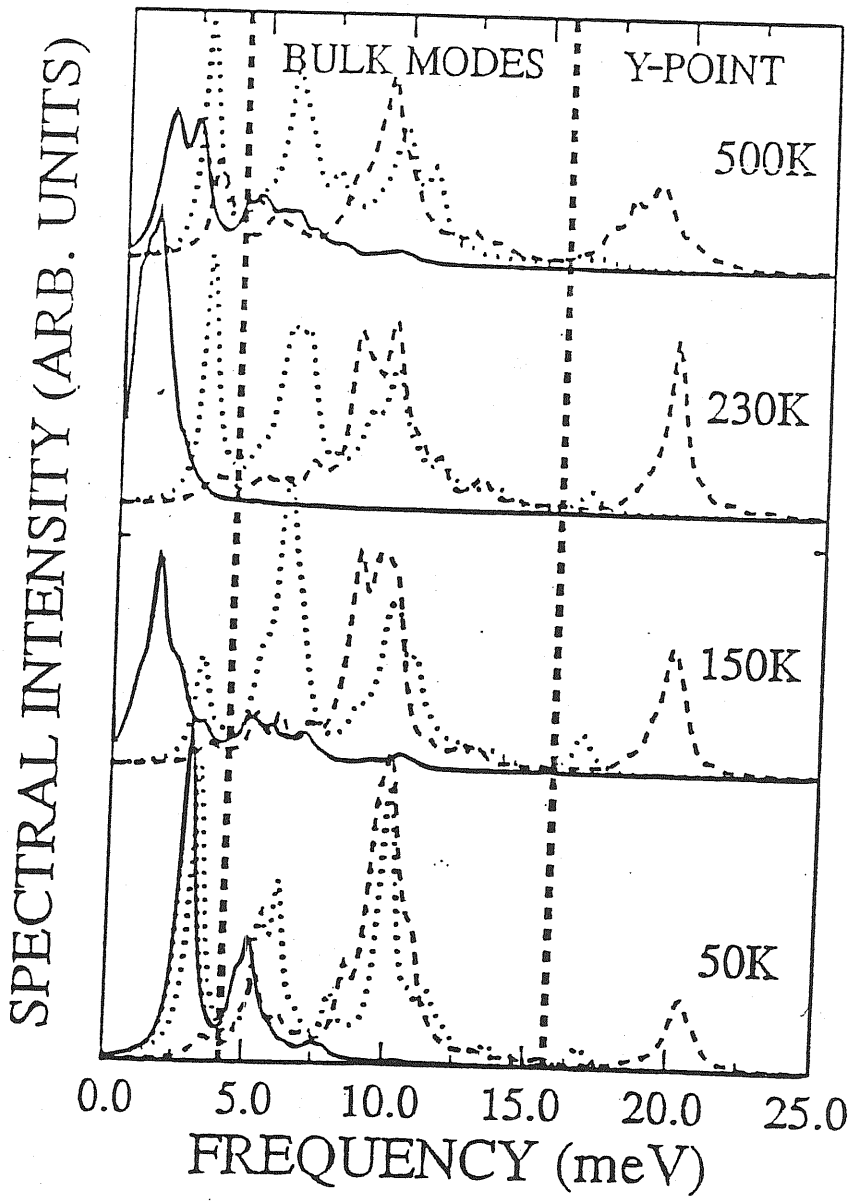

Y-point surface phonon spectral density of Au(110) at various temperatures for directions x (solid), y (dotted) and z (dashed). Note the softening of the x (shear horizontal) mode at low frequency, and the high-frequency z (shear vertical) modes.

simulation is not designed for the study of this transition, which involves large displacements and long simulation runs. Only the low-temperature transition can therefore play a role in our case. Its main signature in the spectrum of Fig.4.1 is an anomalous softening of the shear-horizontal low-frequency branch near the Y point for $T \sim T_c$. The nature of this whole branch consists precisely of motions of the top rows along their own direction (x).

The high-temperature mode H_1 is also remarkably temperature-dependent. At $\vec{k} = 0$, it exhibits a steady downwards shift from $\sim 20meV$ at $50K$ to $\sim 18meV$ at $500K$, without any apparent connection with the sliding transition. Since bulk anharmonicities are still irrelevant at 500K, this softening must be attributed to strong intrinsic surface anharmonicities. This fact seems to contrast the usual notion that stiff systems are also rather harmonic. We speculate that the reason why this particular surface mode is also very anharmonic should be connected with the possible decay into a pair of bulk-like modes whose frequencies add up to 20meV. Interestingly, Fig.4.3b shows that (at least at the Y point) there is a large spectral density of bulk-like modes around 10meV, which provides some support for this idea.

Chapter 5

Electron Energy Loss Spectroscopy and Surface Phonons of Au(110)

The anomalous high-frequency mode H_1 lies well above the bulk continuum, and should be easily detectable, by either inelastic He- scattering or by electron-energy-loss spectroscopy (EELS). Pursuing further this last possibility, we have attempted a calculation of the $\vec{k} = 0$ (dipole) EELS spectrum based on our simulation data.

A complete description of the inelastic electron scattering requires an understanding of both the scattering process and the dynamics of the surface. Lattice-dynamical calculations have used a number of calculational schemes such as the Green's-function techniques [38-40], continued-fraction method [38], and finite slabs [41-42]. In the case of ordered adsorbate overlayers, direct information concerning the adsorption-site configuration may be obtained in some cases, from a simple symmetry analysis based on

selection rules for dipole scattering [43].

5.1 Theory

The inelastic scattering of low-energy electrons from surfaces can be described by two scattering mechanisms which can be conveniently discerned by the appropriate scattering geometry [44]. These are dipole scattering from the long-range Coulomb interactions between the incident electron and the electric field fluctuations associated with the surface modes, and impact scattering from short-range interactions with the atomic potentials of the surface atoms. Dipole scattering is associated with an intensity distribution with peaks sharply in the specular direction, corresponding to very small wave-vector transfer parallel to the surface, $Q_{\parallel}$ [38]. In contrast, impact scattering is typically associated with a broad angular distribution and gives a small contribution in the specular direction in comparison to dipole-excited modes [44].

The theory of dipole scattering from surfaces is well established [38,45]. The inelastic cross section obtained in the Born approximation is given by a product of two factors. The first is a kinematic factor which depends on the scattering geometry and is independent of the properties of the substrate. The second factor is related to the correlation function of the charge-density fluctuations in the surface region [46]. In the application to vibrational motion, this factor is the spectral function $S(\omega)$ for the dipole-dipole correlation function which is defined as

$$S(\omega) = \frac{1}{N} \int \frac{dt}{2\pi} \exp(i\omega t) < \mu_z(t)\mu_z(0) >, \qquad (5.1)$$

where μ_z is the normal component of the total dynamic dipole moment, N is the number of surface primitive cells, and the angular brackets denote a statistical average.

The semi-infinite crystal may be regarded as a system of planes of nuclei, with each plane parallel to the surface. Let the position of each atom be denoted by $R(\mathbf{L})$, where $\mathbf{L} = (\mathbf{L}_\parallel, L_z)$, $\mathbf{L}_\parallel$ is a vector parallel to the surface directed to a particular unit cell, L_z denotes a particular atomic layer. The relation between the normal component of the total dipole moment and the displacement $\mathbf{u}(\mathbf{L})$ of an atom away from equilibrium is given by the effective charge field $\mathbf{e}^*(\mathbf{L})$ defined by

$$\mu_z = \sum_{\mathbf{L}} \mathbf{e}^*(\mathbf{L}) \cdot \mathbf{u}(\mathbf{L}) \tag{5.2}$$

Due to the translational symmetry of the lattice we have $\mathbf{e}^*(\mathbf{L}) = \mathbf{e}^*(L_z)$. Thus only displacement fields at the $\bar{\Gamma}$ point $\mathbf{Q}_\parallel = 0$ can give rise to a nonzero dipole moment μ_z.

The evaluation of the spectral function $S(\omega)$ thus involves determining a displacement-displacement correlation function. The spectral function $S(\omega)$ can be directly related to a phonon density of states, $g(\omega, \mathbf{v}^*)$, projected onto a normalized effective charge field $\mathbf{v}^*$ as

$$S(\omega) = \frac{\hbar (e^*_{tot})^2}{2M\omega}[1 + n(\omega)]g(\omega, [\mathbf{v}^*(L_z)]), \tag{5.3}$$

where

$$\mathbf{v}^*(L_z) = \frac{\mathbf{v}^*(L_z)}{e^*_{tot}} \tag{5.4}$$

$$e^*_{tot} = [\sum_{L_z} \mathbf{e}^*(L_z)^2]^{1/2} \tag{5.5}$$

Here $n(\omega)$ is the Bose-Einstein distribution factor. In the classical limit it is proportional to $1/\omega$.

The evaluation of the spectral function is facilitated by considering the symmetry of the system. Due to symmetry, displacement fields belonging to different symmetry classes are decoupled. Furthermore, the dipole selection rule states that only the totally symmetric displacement fields at the $\bar{\Gamma}$ point of the surface Brillouin zone (SBZ) are dipole active. This selection rule follows simply from the invariance of the total dynamic dipole moments for all operations belonging to the symmetry group of the system. Thus for the evaluation of the spectral function it is necessary only to consider those displacement fields which are totally symmetric at the $\bar{\Gamma}$ point of the SBZ.

In the modeling of the effective charge field we make the assumption that the effective charges $e^*(L_z)$ are nonzero only for the top three layers. This assumption is based on the fact that the efficient screening by the conduction electrons will limit the dipole activity to the outermost surface layers. Additionally, noting that for mode H_1 the topmost row and the underlying third-layer row vibrate bodily against one another, we further model the dipole activity by the bond-stretch displacements between those two rows only. While this simplification is largely arbitrary, we have also checked that different choices differ only by uninteresting relative shifts of intensity.

The density of states constructed from MD simulations will then consist of a discrete set of peaks located at the eigenfrequencies. The limited energy resolution in measured energy-loss spectra can be described by re-

placing these peaks by a normalized Gaussian distribution with a width given by the experimental resolution. In our numerical work, we have simulated the resolution of the 'instrument' as follows. Let $I(\omega)$ be the contribution from one particular bulk or surface phonon excited in a scattering geometry of interest. Then we use for the loss cross section $I(\omega)$ to be compared with the data

$$I(\omega) = \frac{1}{\pi} \sum_j \frac{I(\omega_j)\Gamma}{(\omega - \omega_j)^2 + \Gamma^2} \tag{5.6}$$

where 2Γ is a measure of the resolution.

5.2 Results and Discussions

The simulation is based on a 16-layer slab, with in-plane (x,y) periodic boundary conditions, and free z-motion. At each temperature, a suitable number of canonical MD steps, usually 2000 (one step=7.14×10^{-15} sec) is allowed for equilibration. Following this, a total of 7000 steps are used for evaluation of the average. In essence, the mean instantaneous modulation of the first third layer spacing is assumed to be proportional to the oscillating macroscopic dipole moment capable of scattering the electron .

Fig.5.1 presents our results for $S(\omega)$ as a function of temperature. We identify two main frequency ranges: bulk frequencies ($\omega < 16$ meV), and high frequencies ($\omega > 16$ meV). The EELS spectra exhibit several strong peaks in the bulk range, the intensity broadening from one to the other with increasing temperature. The overall feature of these low frequency structures represents the surface dipole scattering produced by bulk modes. It is rather strong, and should be fully observable. However, it is neither

Fig.5.1.

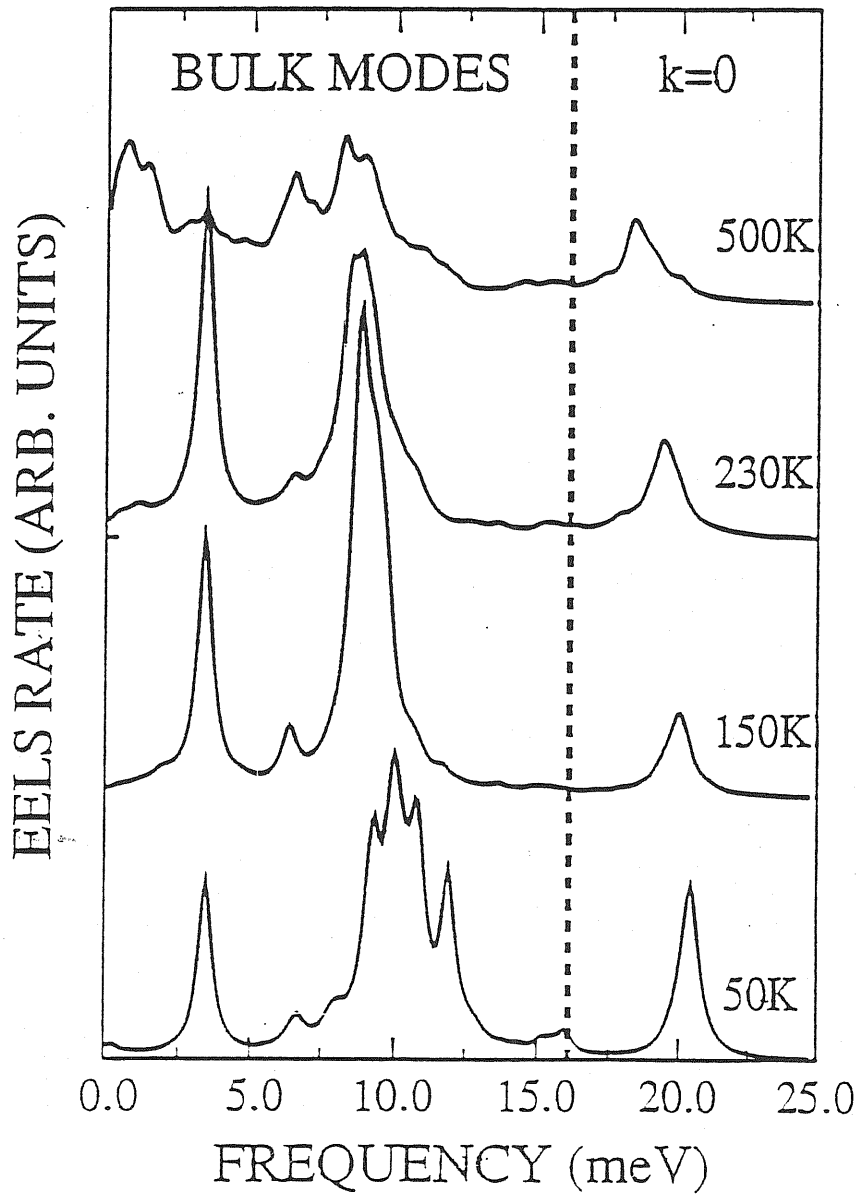

Simulated EELS spectrum of Au(110).

very eventful, nor very much related to the reconstructed structure.

The high frequency modes found in our simulation is the same mode we discussed in the previous chapter,thus the above results constitute a prediction for a high resolution EELS vibrational experiment as a function of temperature.

In summary, we have reported a study, carried out by molecular dynamics, of the temperature-dependent surface dynamics of reconstructed $Au(110)$, as it would appear through inelastic vibrational spectroscopy. We have shown that the missing-row reconstructed Au(110) surface should exhibit anomalous high-frequency modes, directly related to the topmost layer "sinking" relaxation. This feature is expected to be common to all other missing-row reconstructed surfaces, in view of their close structural analogy and very similar underlying physics. Direct observation of these modes has not yet been attempted, and should be considered, particularly by means of EELS.

References

1. See review article by H.Ibach and T.S.Rahman, in Chemistry and Physics of Solid Surfaces, edited by R.Vanselow and R.Howe (Springer-Verlag, New York,1984)

2. S.Lehwald, J.M.Szeftel, H.Ibach, T.S.Rahman and D.L.Mills, Phys. Rev.Lett. 50,518(1983);J.M.Szeftel,S.Lehwald, H.Ibach, T.S.Rahman, J,E.Black, and D.L.Mills, Phys.Rev.Lett. 51,268(1983)

3. R.L.Strong and J.L.Erskine, Phys.Rev.Lett.54,346(1985)

4. See review article by J.P.Toennies, J.Vac.Sci.Technol. A2,1055(1984)

5. G.Brusdeylins, R.B.Doak,and J.P.Toennies, Phys. Rev. Lett. 46,437(1981)

6. R.E.Allen, G.P.Alldredge and F.W. de Wette, Phys.Rev.B4,1648,1661(1971)

7. J.E.Black and R.F.Wallis, Phys.Rev.B29,6972(1984)

8. B.J.Alder and T.E.Wainright, J.Chem. Phys.27,1208(1957);39,459(1959)

9. A.Rahman,Phys.Rev.A136,405(1964)

10. See, for example, M.Parinello and A.Rahman, J.Chem.Phys. 80,860(1984) and references therein.

11. R.Car and M.Parinello, Phys. Rev. Lett. 55,2471(1985)

12. M.Parinello and A.Rahman, Phys. Rev. Lett. 45,1196(1980)

13. C.S.Jayanthi, E.Tosatti, and A.Fasolino, Phys. Rev.B31,470(1985)

14. R.A.Johnson and W.D.Wilson, in Interatomic Potentials and Simulation of Lattice Defects, edited by P.C.Gehlen, J.R.Beeler, and R.I.Jaffee(Plenum, New York,1971)

15. R.A.Johnson, J.Phys.F3,259(1973)

16. M.I.Baskes and C.F. Melius, Phys.Rev.B20,3197(1979)

17. R.B.Doak,U.Harten, and J.P.Toennies, Phys. Rev. Lett. 55,2308(1985).

18. M.S.Daw and M.I.Baskes, Phys. Rev. B29,6443(1984).

19. F. Ercolessi, E. Tosatti and M. Parrinello, *Phys. Rev. Lett.* **57**, 719 (1986); F. Ercolessi, M. Parrinello and E. Tosatti, *Surf. Sci.* **177**, 314 (1986).

20. M.W.Finnis and J.E.Sinclair, Philos. Mag. A50,45(1984).

21. D.Tomanek and k.H.Bennemann, Surf. Sci. 163,503(1985).

22. F.Ercolessi,thesis, international School for Advanced Studies, Trieste, 1986

23. M. Garofalo, E. Tosatti and F. Ercolessi, *Surf. Sci.*, in press (1987).

24. K.-P. Bohnen and K. M. Ho, (to be published).

25. F. Ercolessi, M. Parrinello and E. Tosatti, (to be published).

26. M. S. Daw, *Surf. Sci.* **166**, L161 (1986).

27. W. Moritz and D. Wolf, *Surf. Sci.* **163**, L655 (1985).

28. M. Copel and T. Gustafsson, *Phys. Rev. Lett.* **57**, 723 (1986); M. Copel, P. Fenter and T. Gustafsson, (preprint).

29. G. Binnig, H. Rohrer, Ch. Gerber and E. Weibel, *Surf. Sci.* **131**, L379 (1983).

30. C. M. Chan and M. A. Van Hove, *Surf. Sci.* **171**, 226 (1986).

31. G. L. Kellogg, *Phys. Rev. Lett.* **55**, 2168 (1985).

32. B. E. Hayden, K. C. Prince, P. J. Davie, G. Paolucci and A. M. Bradshaw, *Solid State Commun.* **48**, 325 (1983).

33. S. R. Nagel, A. Rahman and G. S. Grest, *Phys. Rev. Lett.* **47**, 1665 (1981).

34. E. Evans and D. L. Mills, *Phys. Rev. B* **5**, 4126 (1972).

35. D. Wolf, H. Jagodzinski and W. Moritz, *Surf. Sci.* **77**, 265, 283 (1978).

36. J. C. Campuzano, M. S. Foster, G. Jennings, R. F. Willis and W. Unertl, *Phys. Rev. Lett.* **54**, 2684 (1985).

37. M. S. Daw, Proc. 2nd Intern. Conf. on the Structure of Surfaces, Amsterdam, 1987.

38. J.E.Black, in Vibrations at Surfaces, edited by R.Caudano, J.M.Gilles, and A.A.Lucas(Pienum, New York,1982), p.57.

39. T.S.Rahman, D.L.Mills, and J.E.Black, Phys.Rev.B27,4059(1983); D.L.Mills, T.S.Rahman, and J.E.Black, Phys.Rev.B27,4072(1983); T.S.Rahman, D.L.Mills, and J.E.Black, Phys.Rev.Lett.46,1059(1981).

40. M.Persson, Phys.Scr. 29,181(1984).

41. G.Allen and J.Lopez, Surf. Sci. 95,214(1980).

42. V.Bortolani, A.Francchini, F.Nizzoli, and G.Santoro, Solid State Commun. 41,369(1982)

43. R.L.Strong, B.Firey, F.W. de Wette, and J.L.Erskine,Phys.Rev.Lett.54,346(1985)

44. Persson and S.Andersson, Surf.Sci.117,352(1982).

45. J.A.Stroscio, M.Persson, and W.Ho, Phys.Rev.B33,6758(1986).